Human Cryptochrome1 dampens homologous recombination at nightfall

One sentence summary: CCAR2-dependent inhibition of DNA end resection and homologous recombination is controlled by the intrinsic cellular circadian clock

Amador Romero-Franco[1,2], Cintia Checa-Rodríguez[1,2]#, Maikel Castellano-Pozo[1,2], Hector Miras[3], Amadeo Wals[3] and Pablo Huertas[1, 2,*]

[1] Facultad de Biología, Universidad de Sevilla, Sevilla, 41080, Spain

[2] Centro Andaluz de Biología Molecular y Medicina Regenerativa-CABIMER, Universidad de Sevilla-CSIC-Universidad Pablo de Olavide**,** Sevilla, 41092, Spain

[3] Servicios de Oncología Radioterápica y de Radiofísica, Hospital Universitario Virgen Macarena, Sevilla, Spain

Present address: Instituto de Biomedicina de Sevilla-IBiS, Hospital Universitario Virgen del Rocío/CSIC/Universidad de Sevilla, Sevilla, 41013, Spain

*To whom correspondence should be addressed. Tel: +34 954 467 667; Fax: +34 954 461 664; Email: pablo.huertas@cabimer.es

Lead Contact: Pablo Huertas

Keywords: DNA end resection/DNA repair/Homologous recombination/Circadian clock/CCAR2/CRY1

Abstract

The maintenance of genomic stability is essential for cellular and organismal survival and fitness. Thus, when DNA gets damaged, is essential to repair it in the most accurate fashion. Among different DNA lesions, DNA double strand breaks are specially challenging. An exquisite regulatory network reacts to local and global cues to control the choice between different DNA double strand break repair mechanisms to maximize genomic integrity. Such regulation relies mostly at the level of DNA end resection, the initial steps of the homologous recombination repair pathway. On the other hand, most cellular and organismal activities follow a 24 h oscillation known as the circadian cycle. Such repetitive changes are controlled by an intrinsic, molecular clock built-in at the cellular level which core components are the heterodimers BMAL1-CLOCK and CRY-PER. These inherent rhythms control many different aspects of the cellular metabolism, including the fate of many different DNA transactions. Here we have explored the regulation of the choice between different DNA double strand break repair pathways along the circadian cycle. We observed that DNA end resection shows a circadian oscillation, with a peak at dawn followed by a progressive reduction until dusk. Such regulations depend on the cellular levels of the circadian clock core component CRY1. Consequently, repair by homologous recombination mirrors CRY1 expression levels. Such modulation is controlled through the circadian regulation of the anti-resection activity, but not the protein levels, of CCAR2, that limits CtIP-mediated resection preferentially at nightfall. Additionally, such regulation requires a crosstalk between the DNA damage-dependent phosphorylation of CRY1 by the kinase DNA-PK. Finally, such regulation has an impact in cancer progression and response to radiation therapy of specific tumors.

INTRODUCTION

DNA double-strand break (DSB) repair is a critical aspect of cellular biology that has a great impact in different human diseases such as cancer (Jackson and Bartek, 2009). Any DSB can be channelled through different repair pathways, with specific requirements and distinctive outcomes. In general, such pathways can be ascribed mostly to two different families: homology-driven repair (HDR), that take advantage of the presence of intact copies of the broken sequences to use as a template, especially the sister chromatid; and non-homologous end-joining (NHEJ), the simple ligation of two DNA ends with little or even no processing (Chang et al., 2017; Jasin and Rothstein, 2013; Ranjha et al., 2018). Both can result in either faithful or mistaken repair, thus the choice between them is tightly regulated and respond to both local and global cellular cues. The best characterized regulatory step for DSB repair pathway choice is the activation of DNA end resection, a degradation of one strand of the broken DNA to create long tails of 3' protruding ssDNA (Cejka, 2015; Symington, 2016). Resection regulation relies mostly on the control of a single core resection factor, CtIP, that integrates multiple of those signals in the form of specific interactions and/or post-translational modifications (Makharashvili and Paull, 2015; Mozaffari et al., 2021). Once CtIP is activated, resection ensues and NHEJ is reduced. On the contrary, if CtIP is blocked, resection is hampered and NHEJ prevails. Among many different other factors, CCAR2 function as a CtIP antagonist in resection regulation (López-Saavedra et al., 2016), acting as a downstream effector of the Shieldin complex (Iyera et al., 2022). Both proteins interact constitutively, but in some particular circumstances the eviction of CCAR2 allows CtIP unleashing, thus favouring a pro-resection setting (López-Saavedra et al., 2016).

Another essential biological process is the circadian rhythm, a series of periodic oscillations that follow the day/night cycle (Stratmann and Schibler, 2006). Its presence is conserved throughout the whole photosensitive spectrum of living organisms, ranging from free living unicellular algae to complex multicellular organism such as humans, albeit the circadian machinery has widely changed across evolution (Bhadra et al., 2017). In synthesis, the circadian clock works as a built-in 24-hour oscillator that acts in a two-tier fashion: an intrinsic cellular circadian clock with a roughly 24 h period that can be synchronized in response to the external light, a process commonly regarded as photoentrainment (Stratmann and Schibler, 2006). In mammals, at the molecular level, the transcription factors BMAL1 and CLOCK stimulates the expression of the genes that code for the Period (PER1-3) and Cryptochrome (CRY1-2) families during the activation

phase, that in humans coincide with daylight hours. Then, PER and CRY heterodimers translocate into the nucleus where CRY negatively affect the transcriptional activity of BMAL1/CLOCK, mainly during night hours (Takahashi, 2017). Thus, a recurrent oscillation is created by sequential transcriptional activation/repression waves. Additional accessory loops have been characterized in the circadian clock, but the pair of heterodimers BMAL1/CLOCK and PER/CRY build the core cellular oscillator (Brown et al., 2012).

Here we show that DNA end resection, the licensing step of HDR, is regulated in a circadian fashion. Indeed, resection activity peaks at dawn and slowly decrease during the day, followed by an increase during the night. Such regulation relies specifically in the circadian factor CRY1, reacting at its presence or absence. Mechanistically CRY1 is recruited to sites of DSB and reinforce the inhibitory effect of CCAR2 over CtIP by potentiating CCAR2 retention on damaged chromatin. Furthermore, the DNA Damage Response (DDR) kinase DNA-PK finetunes this circadian effect. Upon DSBs appearance, CRY1 is recruited to damaged chromatin, then phosphorylation by DNA-PK allows it retention at sites of damaged DNA. This locks CCAR2 at those sites, curbing CtIP activity. This negative modulation maximizes around nightfall, when CRY1 levels peak, whereas the absence of this protein at dawn breaks this regulatory circuit, hence licencing DNA end processing. Finally, this fine regulation of end resection affects the ability of cells to deal with DNA damaging agents *in vitro*, but also in cancer treatments setups.

Material and Methods

Cell lines and growth conditions

U2OS cells and MEFs were grown in high glucose DMEM (Sigma-Aldrich) supplemented with 10% foetal bovine serum (Sigma-Aldrich), 2 mM L-glutamine (Sigma-Aldrich), 100 units/ml penicillin, and 100 µg/ml streptomycin (Sigma-Aldrich). U2OS cells stably expressing GFP-CtIP, GFP-CCAR2, Cherry-CtIP and Cherry-MDC1 were grown in a standard medium supplemented with 0.5 mg/mL G418 (Gibco, 15140122). U2OS cells harbouring a single copy of the reporter constructs DR-GFP, SA-GFP and EJ5-GFP were grown in a standard medium supplemented with 1 µg/mL puromycin (Sigma, P8833).

RPE1 cells were grown in high glucose DMEM/F-12 medium (Sigma-Aldrich) supplemented with 10% foetal bovine serum (Sigma-Aldrich), 2 mM L-glutamine (Sigma-Aldrich), 100 units/ml penicillin, and 100 µg/ml streptomycin (Sigma-Aldrich).

RPE1 cells stably expressing shRNAs against CtIP, CCAR2 and a control sequence (shScr) were grown in this medium supplemented with 5μg/mL puromycin (Sigma, P8833).

To inhibit DNA-PK we used NU7441(SelleckChem) for 1 hr prior irradiation. To stabilize CRY1, cells were pretreated with KL001 (Sigma) for 24 hrs prior the relevant experiment.

siRNAs, plasmids, and transfections

siRNA duplexes were obtained from Sigma-Aldrich or Dharmacon (Supplementary Table S1) and were reversely transfected using RNAiMax Lipofectamine Reagent Mix (Life Technologies), according to the manufacturer's instructions. Plasmid transfection was carried out using FuGENE 6 Transfection Reagent (Promega) according to the manufacturer's protocol.

Circadian synchronization experiments

Circadian synchronization was performed by treating cells with either 1 μM of Dexamethasone (Sigma), or 10 μM of Forskolin (Sigma) or mock treated with EtOH or DMSO as a control, respectively, for 2 hours. Release from synchronization was performed by exchanging the medium with fresh one.

Immunoprecipitation

U2OS cells were harvested in lysis buffer (50 mM Tris–HCl, pH 7.5, 50mM NaCl, 1 mM EDTA, 0.2 % Triton X-100, 1X protease inhibitors (Roche), 1X phosphatase inhibitor cocktail 1 (Sigma)) and incubated for 30 min on ice with Benzonase (100 U/mL). Protein extracts (500 μg-1 mg) were then subjected to preclearing with 20 μL of either magnetic protein G (for Rabbit antibodies) or Protein A (for Mouse antibodies) Dynabeads (Invitrogen) for 1 hour at 4ºC. Then, precleared extracts were incubated overnight with 0.5 μg of CRY1 antibody (Rabbit, A302-614A), 1 μg of CCAR2 antibody (Rabbit, A300-433A-1), 1.5 μL of CCAR2 antibody (Mouse, 5857) or the equivalent amount of IgG (Mouse or Rabbit) as the negative control. Subsequently, extracts were incubated with the corresponding magnetic protein beads and after that they were washed three times with lysis buffer with 0.02% of Triton X-100. The precipitate was eluted in 30 μl of Laemmli buffer 2X. The antibodies used for immunoprecipitation can be found on Supplementary Table S2.

Immunofluorescence and microscopy

For foci visualization, cells were seeded on 12 mm coverslips, and after the different treatments, cell were washed once with PBS before following the immunofluorescence procedure.

For RPA and BRCA1 foci analysis, cells were pre-extracted with Pre-extraction Buffer (25 mM Tris–HCl, pH 7.5, 50 mM NaCl, 1 mM EDTA, 3 mM $MgCl_2$, 300 mM sucrose, and 0.2% Triton X-100) for 5 min on ice. Then, cells were fixed on ice with 4% paraformaldehyde (w/v) in PBS for 20 min. For RIF1, 53BP1 and γH2AX foci analysis, cells were treated for 20 min on ice with 4% paraformaldehyde (w/v) in PBS, and after two washes with PBS 1X, they were permeabilized with 0.25% Triton X-100 in PBS. For RAD51 foci analysis, cells were pre-extracted with 0.1% Triton X-100 in PBS for 5 min on ice. Then, cells were fixed on ice with 4% paraformaldehyde (w/v) in PBS for 20 min on ice.

In all cases, following two washes with PBS, cells were blocked for 1 h with 1% BSA in PBS, co-stained with the appropriate primary antibodies (Supplementary Table S2) in blocking solution overnight at 4 °C, washed again with PBS and then co-immunostained with the appropriate secondary antibodies (Supplementary Table S3) in blocking buffer. After washing with PBS and dehydration with 100% ethanol, coverslips were mounted into glass slides using Vectashield mounting medium with DAPI (Vector Laboratories). In the case of QIBC experiments, cells were stained with 0.5 µg/mL DAPI in PBS for 5 min prior to drying with ethanol and were mounted using Vectashield mounting medium without DAPI (Vector Laboratories). Images were acquired and analysed using a Leica fluorescence microscope. Foci analysis formation was performed using ImageJ.

Single-molecule analysis of resection tracks

To measure the length of the resected DNA fragments SMART (single-molecule analysis of resection tracks) assay was performed or directly lysing and stretching the DNA on coverslip (SMART-tilt) (Altieri et al., 2020). U2OS cells were grown in the presence of 32 µM CldU (Sigma, C6891) for 24 h. They were then irradiated (10 Gy) for 1 h at 37°C and harvested using Trypsin. Cells were centrifuged at 500 g for 3 min at 4 ºC, resuspended in PBS and mixed in a 1:8 proportion with unlabelled cells. For DNA stretching, 2.5 µl of this mix were lysed using a spreading buffer (50 mM EDTA, 0.5%

SDS, 200 mM Tris-HCl pH 7.4) to later stretch the nucleic acid fibers on silanized slides (Sigma, S4651), tilting the slides to a 15°. After air-drying the DNA fibers for 10 min, they were fixed in 3:1 methanol/acetic acid at -20 ºC for 15 min. Slides were then washed twice in PBS, incubated in 70% ethanol overnight at 4ºC and washed twice again in PBS. For immunodetection, samples were blocked with 5% BSA (Sigma, A4503) in PBS for 30 min at room temperature (RT) and incubated with anti-BrdU/CldU (Abcam, ab6326) diluted in blocking buffer for 1 h at 37ºC. Slides were washed with PBS twice and incubated with the fluorescent secondary antibody (Alexa Fluor 488 anti-rat, Molecular Probes A-11006) diluted in blocking buffer for 1 h at RT. Finally, samples were washed twice in PBS, dried and mounted with ProLong Gold Antifade Reagent (Molecular Probes, P36930). DNA fibers images were acquired with a Leica Thunder Microscope with automatized stage and a 63X oil immersion objective. For each experiment, at least 100 DNA fibers were measured using the Fiji (ImageJ) image software analysis.

SDS-PAGE and western blot analysis

Protein extracts were prepared in 2X Laemmli buffer (4% SDS, 20% glycerol, 125 mM Tris–HCl, pH 6.8) and boiled at 100 ºC for 5 min. Then, samples were resolved by SDS–PAGE and transferred to Amersham™ Protran™ Premium NC nitrocellulose membranes (Cytiva Life Sciences). Membranes were blocked with 5% Skim Milk (Difco) in 0.1% Tween-20, 0.01% Sodium Azide supplemented 1X TBS. After that, membranes were blotted with the appropriate primary antibody (Supplementary Table S2) and infrared dyed secondary antibodies (Supplementary Table S3) diluted in Odyssey Blocking Buffer (LI-COR) supplemented with 0.1% Tween-20 and 0.01% Sodium Azide. Membranes were air-dried in the dark and scanned in an Odyssey Infrared Imaging System (LI-COR), and images were analysed with Image Studio software (LI-COR).

Cell cycle analysis

Cells were fixed with cold 70% ethanol for at least 2 hours, incubated with 250 µg/ml RNase A (Sigma Aldrich) and 10 µg/ml propidium iodide (Sigma Aldrich) at 37 °C for 30 min and analysed with a LSRFortessa™ Cell Analyzer (BD) Flow Cytometer. Cell cycle distribution data were further analysed using ModFit LT 5.0 software (Verity Software House Inc).

HR and NHEJ analysis

U2OS cells bearing a single copy integration of the reporters DR-GFP (Gene conversion) or SA-GFP (SSA) were used to analyse the different DSB repair pathways. In both cases, 60.000 cells were plated in 6-well plates in duplicate. One day after seeding, cells were transfected with the indicated siRNA or plasmids. The next day, each duplicate culture was infected with lentiviral particles containing I-SceI–BFP expression construct at MOI 10 using 8 µg/ml polybrene in 2 ml of DMEM. Then, cells were left to grow for an additional 24 h before changing the medium for fresh DMEM. 48 h after viral transduction, cells were washed with PBS, trypsinized, neutralized with DMEM, centrifuged for 3 min at 600 g, and collected by centrifugation and resuspended in 300 µl of PBS. Samples were analysed with a LSRFortessa™ Cell Analyzer (BD) Flow Cytometer.

UV laser micro-irradiation

For the analysis of laser-localized fusion proteins, cells were seeded on µ-slide glass bottom plates (Ibidi). Experiments were imaged with an ORCA Flash 4.0 sCMOS camera (Hamamatsu) using a Yokogawa CSU-W1 Confocal Scanner Unit (Gataca Systems) in an Axio Observer 7 microscope (Zeiss) at 37 ºC and 5% CO_2 conditions. Laser microirradiation was performed using a laser output of 20% power of a 355nm laser line (10mW; 19kHz, iLAS 3 Gataca Systems) through a UV-transmitting 100-X oil immersion objective (Zeiss). Laser stripes were created at the cell nucleus with a pixel size of 1, and 2 iterations per stripe using MetaXpress software (Molecular Devices). After irradiation, GFP or Cherry tagged protein accumulation at laser tracks was recorded at the indicated times. Signal intensity was measured using Fiji (ImageJ) by subtracting pre-irradiation signal to each time-point and represented as arbitrary units (a.u.).

Clonogenic cell survival assays

Clonogenic survival assays were carried out seeding 500 cells in 6-well plates triplicates 24 hours prior to treatment. DSBs were produced by ionizing radiation (IR) or by acute treatment with topoisomerase inhibitor etoposide (VP16; Sigma). For IR, cells were exposed to 2 or 4 Gy or mock treated. In the case of VP16 treatments, cells were incubated for 1 h with 5 or 10 µM of the drug or vehicle (DMSO) as control. After two washes with PBS, a fresh medium was added, and cells were incubated at 37 °C for 7–14 days to allow colony formation. Afterward, cells were stained and visualized in the solution of 0.5% Crystal Violet (Merck) and 20% ethanol (Merck). Once the colonies

were stained, this solution was removed, and plates were washed with distilled water. The portion of surviving colonies at each dose was calculated by dividing the average number of visible colonies in treated versus control dishes.

ICGC data retrieval and analysis

Patient sets were retrieved from the International Cancer Genome Consortium (ICGC) Data Portal TCGA Breast Cancer (BRCA) datasets. CRY1 and CCAR2 expression levels, survival and radiation therapy information from each donor were obtained using the UCSC Xena web tool.

Patient data

Survival data was obtained from the Radiotherapy Service at the University Hospital Virgen Macarena, Seville Spain, from all patients treated with radiotherapy as a primary form of treatment between May 2018 to October 2022. In all cases, in addition to the type of cancer, the gender and age (Supplementary Table S4), the date of treatment initiation, the date of the last known interaction (either the death of the patient or the last known follow up), and approximate time of irradiation was recorded. Each patient was always treated at the same time of the day. Patients were split in two cohorts, according to the time of irradiation, those treated in the first half of the day (8:00 to 14:00; morning) or the second half (14:00 to 20:00).

RESULTS

DNA end resection shows a circadian cycle

As mentioned, all animal cells have a built-in circadian oscillator of approximately 24 h. However, *in vitro* grown mammalian cell cultures lack the resetting ability of cells in the whole animals, as they cannot sense light. Luckily, it is simple to reset the circadian clock in cell cultures by the addition of different drugs (Balsalobre et al., 2000; Izumo et al., 2006). To study if DNA end resection follows a circadian pattern, we synchronized U2OS cells with either Dexamethasone (DEX) or Forskolin (FSK) for two hours, resetting the internal clock to the equivalent of dawn (Fig.1A). Then, we released them by washing the medium and irradiated them to induce DSBs at fixed time points that represent different times of the day (Fig. 1A). A control treated with the vehicle instead of the synchronizing drug, therefore maintaining an asynchronous population, was prepared in parallel. Circadian synchronization was followed by the

levels of the core circadian components CRY1 and CRY2, that peak at sunset (Suppl. Fig. 1A). Then, we analysed DNA end resection by checking the formation of RPA foci by immunofluorescence upon 10 Gy of irradiation. As seen in figure 1B, U2OS cells synchronized with DEX (blue line) showed a marked oscillation in resection proficiency, clearly distinct to the observed in the control treated with the vehicle EtOH (red line; see Suppl. Fig. 1B for representative images). Whereas at noon and midnight the number of cells actively resecting was like the control, a marked reduction was readily observed at times equivalent to dusk. Moreover, at sunrise resection was slightly elevated when compared with the asynchronous culture. Similar results were observed when circadian synchronization was achieved by adding FSK when compared with the mock treatment with DMSO (Fig. 1C, Suppl. Fig. 1C). Furthermore, this oscillation was also evident in the primary human cell line RPE1 (Fig. 1D, Suppl. Fig. 1D) or in mice MEFs (Fig. 1E, Suppl. Fig. 1E) when compared with an asynchronous population (from this point onward, only a single asynchronous sample was taken and represented as a dashed line). Cell cycle is a major regulator of DNA end resection (Cejka, 2015; Ferretti et al., 2013; Mozaffari et al., 2021; Symington, 2016) and both the circadian and the cell cycles are known to crosstalk (Gaucher et al., 2018). However, our results could not be attributed to changes in cell cycle distribution, as it was not affected by circadian synchronization in our experimental setups (Suppl. Fig. 1F-H). To determine if the circadian rhythm controlled only the initiation of DNA end resection or if, instead, affected also the processivity of the process we measured the actual length of resected DNA tracts at different positions on the circadian cycle (Fig. 1F). We observed that at sunrise, in agreement with a more permissive environment for resection, the length of DNA resected was longer than the asynchronous control (compare 24 h with the control). On the contrary, at sunset resection was limited, and the extension of the resected DNA greatly diminished. Resection is heavily controlled by multiple signals (Cejka, 2015; Symington, 2016), but a well-defined modulatory axis is determined by the antagonistic relationship between the pro-resection factor BRCA1 and the anti-resection complex Shieldin (Chapman et al., 2013; Escribano-Díaz et al., 2013; Di Virgilio et al., 2013). So, to reinforce the idea that resection showed circadian oscillations, we then analysed the recruitment of BRCA1 and the Shieldin subunit RIF1 1h after the irradiation at different times of the circadian cycle. In agreement with our previous results, we observed that BRCA1 was more avidly recruited at sunrise whereas its localization was limited at sunset (Fig. 1G; Suppl. Fig 1I). On the contrary, RIF1 showed the opposite recruitment pattern (Fig. 1H; Suppl. Fig 1J). Finally, we

analysed the recruitment of the recombinase RAD51 to breaks induced at different circadian times. In this case, as RAD51 recruitment is a slower process, we observed its recruitment three hours after DSB formation. In agreement with our previous data, breaks induced at dusk were less likely to engage RAD51 than those created at dawn (Fig. 1I; Suppl. Fig 1K). Thus, we conclude that the circadian cycle in humans creates a more permissive environment for resection early in the morning, but it is partially restricted at dusk.

DNA end resection reacts to CRY1 levels

The inborn cellular circadian clock is controlled by the alternative predominance of the heterodimers BMAL1-CLOCK, that peak at dawn, and CRY-PER, that are mostly expressed at dusk (Takahashi, 2017). Accessory factors finetune the day-night rhythm. We wondered if the circadian oscillation of DNA end resection could be attributed to the protein levels of any of those factors. We took advantage of our previously published results in which we tested the effect of depletion of all human genes in the balance between HR and NHEJ, a screening that rendered the isolation of resection regulators (Lopez-Saavedra et al., 2016). Interestingly, only CRY1 depletion skewed the balance between DSB repair pathways in a way that was compatible with our observed DNA resection circadian oscillation, i.e., an increase in resection/recombination when its expression was reduced. Thus, we decided to test if resection proficiency was reacting directly to CRY1 levels. In agreement with our screening results, and along the same lines of our observed resection increase at sunrise, depletion of CRY1 on its own stimulates DNA end resection upon irradiation and such effect was complemented by ectopic CRY1 expression, discarding any off-target effect caused by the siRNA (Fig. 2A; Suppl. Fig. 2A for depletion levels). Similar results were observed in other cell lines, such as RPE1 and MEFs (Suppl. Fig. 2B-C). Strikingly, CRY1 loss does not abolish the circadian cycle, as its role is taken over by its paralog CRY2, but only shortens it by about 1 h (Baggs et al., 2009). Thus, the fact that CRY1 depletion shows such a marked effect in resection stimulation, like the resection observed at sunrise, strongly suggest that is specifically CRY1, and not the rest of the circadian built-in clock, what modulates this process. Moreover, in stark contrast CRY2 depletion did not cause an RPA foci defect upon irradiation whereas depletion of any PER paralogue showed a reduction in DNA end resection (Suppl. Fig. 2D), reinforcing our hypothesis that CRY1 acts independently of other circadian proteins in this regulatory role of end processing. Of note, this effect was

underestimated, as CRY1 depletion increased the number of G1 cells (Suppl. Fig. 2E-F), a position on the cell cycle that is mostly refractory to DNA end resection. To minimize this cell cycle effect, we repeated the immunofluorescence and analysed RPA foci determining the cell cycle phases by QIBC, using DAPI signal as a surrogate for cell cycle progression. As shown in figure 2B, CRY1 depletion increased the average number of RPA foci (above the horizontal dashed line) in S/G2 cells (right of the vertical dashed line). Therefore, our data suggest that CRY1 downregulation facilitates resection in S/G2, when resection naturally occurs. Overexpression of CRY1 in cells transfected with a control siRNA reduced the amount of RPA foci upon DNA damage (Fig. 2A). To confirm this effect, we repeated the experiment in cells overexpressing human CRY1 but not transfected with any siRNA (Fig. 2C; Suppl. Fig 2G for representative images and 2H for expression levels) or we treated cells briefly with KL001, a drug specifically designed to stabilize CRY1 (Hirota et al., 2012) (Fig. 2D; Suppl. Fig. 2I for expression levels and 2J for representative images). Thus, we conclude that we can artificially mimic the sunrise or sunset condition by either depleting CRY1 or overexpressing/stabilizing CRY1, respectively. We decided to take advantage of this experimental setup to test if DSB repair pathways efficiency were affected by CRY1 levels. Indeed, low levels of CRY1 stimulate homologous recombination, both Rad51-dependent gene conversion and Rad51-independent Single Strand Annealing (Fig. 2E-F). Strikingly, this did not cause a reduction in NHEJ (Fig. 2G). Conversely, high levels of CRY1 hampered homology directed repair (Fig. 2H-I). In agreement with this effect in recombination, RAD51 recruitment to DSB, measured as RAD51 foci, readily react to CRY1 levels (Fig. 2J-K and Suppl. Fig. 2K-L). Strikingly, the foci formation of components of the Shieldin complex were affected by CRY1 expressions levels (Fig. 2L-M and Suppl. Fig. 2M-N), with a opposite pattern of RPA foci formation.

Circadian regulation of resection relies in controlling the antagonist relationship between CtIP and CCAR2

Thus, resection and homologous recombination inversely reacts to the oscillations of CRY1 during the circadian cycle. So, to gain insight on the molecular mechanism behind the circadian control of DNA end resection, we first decided to test the effect of the depletion of the core resection factor CtIP in cells upon circadian synchronization. CtIP acts as a nexus that integrates multiple signals to control DNA end processing (Makharashvili and Paull, 2015; Mozaffari et al., 2021). As expected, CtIP depletion

reduced resection efficiency, measured by RPA foci formation when compared with siRNA control transfected cells (Fig. 3A; Suppl. Fig 3A for representative images). Strikingly, CtIP downregulation not only decreased resection, but mostly abolished the circadian oscillations of the process, suggesting that such regulation might, indeed, relies in controlling this protein. This agrees with our previous results that suggested that this modulation takes place mainly at the resection level. In fact, at dusk resection levels on control cells resemble closely those observed upon CtIP depletion. Therefore, we hypothesized that at sunset, resection was limited to a degree compatible with an inhibition of CtIP.

CtIP is known to suffer a tight regulation at many different levels, including protein levels, mRNA stability, post-translational modifications, but also by the direct interaction with multiple proteins, including pro-resection factors such as BRCA1 or antagonists such as CCAR2 (Lopez-Saavedra et al., 2016; Makharashvili and Paull, 2015; Mozaffari et al., 2021). So, we reasoned that an inhibition of resection at sunset, when CRY1 peaks, would agree with a peak of activity of a resection antagonist such as CCAR2. Strikingly, CCAR2 is already linked with the regulation of circadian rhythms (Chini et al., 2013; Magni et al., 2018). Interestingly, CCAR2 depletion also abolished circadian oscillation of DNA end processing, but in this case allowing fully active resection at any given time of the day/night cycle (Fig. 3A; Suppl. Fig. 3A). Thus, as expected by the lack of a resection inhibitor, RPA foci went up specifically at dusk, indicating that in the absence of CCAR2 resection cannot be limited at any point of the circadian cycle. Importantly, despite many circadian-mediated regulation happening by controlling the transcription of target genes, neither CCAR2 nor CtIP protein levels change during the circadian cycle, arguing against the idea that a simple transcriptional control of these proteins is behind this regulation (Suppl. Fig. 3B). In agreement with this idea, CCAR2 depletion was completely epistatic over both CRY1 depletion and CRY1 overexpression, reinforcing the idea that CRY1 acts through stimulation of CCAR2 to restrict resection (Fig. 3B-C; Suppl. Fig. 3C-E). This epistatic effect cannot be attributed to large cell cycle changes (Suppl. Fig. 3F). This fits with the idea that is the circadian oscillation of CRY1 itself, and not the whole intrinsic circadian oscillation, what controls resection and recombination. Thus, we wondered if CRY1 protein might directly affects CCAR2 via a physical interaction. Strikingly, CCAR2 and CRY1 physically interact in a constitutive fashion, i.e. regardless of the exposure to IR (Fig. 3D). As published, CCAR2 and CtIP also interact constitutively (Lopez-Saavedra et al., 2016). Thus, albeit we could not co-

immunoprecipitate CtIP with CRY1 in this experiment, we wondered if CtIP might affect the pairwise interactions between CRY1 and CCAR2. Indeed, CtIP depletion reduces the interaction between the other two proteins (Fig. 3E), suggesting that all three proteins might interact together.

Considering this interaction, we wondered if CRY1 itself was recruited to sites of chromosome breaks as it has been described for both CtIP and CCAR2 (Lopez-Saavedra et al., 2016). Indeed, using a GFP-CRY1 we observed a fast accumulation of this protein at DSBs by laser microirradiation with an even faster kinetic than the early DDR factor MDC1, tagged with Cherry (Fig. 3F; Suppl. movies 1 and 2), arguing to a role of CRY1 controlling CtIP-mediated resection together with CCAR2 directly on damaged chromatin. We previously showed that CCAR2 interacts with CtIP, and upon the appearance of DSBs resection controls CtIP recruitment and spreading from the breaks (Lopez-Saavedra et al., 2016). In less permissive conditions for resection, CCAR2 is recruited to and maintained at DSBs, where is phosphorylated by ATM to block the DNA end processing (López-Saavedra et al., 2016). On the contrary, in resection-proficient conditions it is evicted from the DNA (López-Saavedra et al., 2016). Considering our observations with CRY1, we wondered if could be acting by regulating CCAR2 retention/eviction from sites of damaged chromatin. Strikingly, phosphorylated CCAR2 recruitment/retention was diminished if CRY1 was downregulated, as observed by the fraction bound to chromatin upon DNA damage induction (Fig. 3G) and retained by immunofluorescence upon pre-extraction (Fig. 3H). Then, we checked CCAR2 eviction from the vicinity of the damaged DNA by laser microirradiation, that can be observed as a negative signal upon known as an anti-stripe (Lopez-Saavedra et al., 2016). Interestingly, CRY1 depletion increases the formation of CCAR2 anti-stripes 7-fold (Fig. 3I, see white arrow for an example of a laser-induced anti-stripe), explaining why resection might be favoured in such conditions. Furthermore, not only the number of cells showing antistripes was increased upon CRY1 depletion, but quantification of the remaining signal at the laser-induced antistripes showed a stronger reduction of the CCAR2 signal (Fig. 3J), agreeing with a reduced capacity to retain the protein at sites of DSBs. On the contrary, when CtIP was downregulated even those fewer cells that showed antistripes still maintain a significant proportion of the GFP signal, arguing that there is some CCAR2 eviction, but a considerable fraction of the protein is still retained (Fig. 3J). Then, we tested if CtIP recruitment/retention to laser lines responded to CRY1 levels *in vivo*. Cells transfected with a control siRNA accumulate quickly, within minutes, GFP-

CtIP laser stripes (Fig. 3K, Suppl. movie 3). All cells in the population showed a quite homogenous response. However, when CRY1 was depleted, we observed that GFP-CtIP accumulation was stronger and at a faster rate (Fig. 3K and Suppl. movie 4). Again, such increase agrees with a more permissive environment for resection and can account for the increased resection when CRY1 is naturally low at dawn. The opposite effect was observed upon CRY1 overexpression using a GFP-tagged version of the protein, that causes a reduction on the recruitment of Cherry-CtIP at laser lines, most likely mimicking what happens at dusk (Fig. 3L; Suppl. movies 5 and 6). Thus, CRY1 levels control the retention or eviction of CCAR2, a requisite to unleash CtIP and allow DNA end resection.

DNA double strand break repair is modulated by the phosphorylation of CRY1 by DNA-PK kinase activity

So, our data fit with a model in which CRY1 presence reinforces the antagonistic effect of CCAR2 over CtIP, stabilizing CCAR2 presence on damaged chromatin hence blocking CtIP release and resection. However, and differently of the cell cycle regulation of resection, this is not an all or nothing mechanism. So, we hypothesized that even when CRY1 levels are high, namely at dusk, there must be a mechanism that allows some resection and that this might be more finely regulated. Thus, we decided to analyse further how the DDR finetuned the circadian oscillations of DNA end resection. Previously, CRY1 itself has been shown to be a substrate of the DDR, specifically to be phosphorylated by the NHEJ kinase DNA-PK at three residues (Gao et al., 2013), that are conserved in mammals but no other vertebrates. Interestingly, this phosphorylation sites are also absent in CRY2. Considering its anti-resection and pro-NHEJ role, it made sense that such phosphorylation stimulates CRY1-mediated inhibition of CtIP-mediated resection. Thus, we decided to analyse the effect of such modification on the modulation of DNA end resection and recombination along the light/dark cycle. First, we tested if DNA-PK-mediated phosphorylation was required for the inhibitory effect of CRY1 over resection. Indeed, ectopic expression of human CRY1 or its stabilization with KL001 hampered DNA end processing only if DNA-PK was active (Fig. 4A-B; Suppl. Fig. 4A-B for representative images). CRY1 has been shown to be phosphorylated at three specific sites. So, to test if this effect was direct, we checked the effect of the overexpression of a CRY1 version that cannot be phosphorylated by DNA-PK (CRY1-3A) or that mimicked constitutive phosphorylation (CRY1-3E) in resection in the presence or absence of DNA-PK inhibitor. As shown in figure 4C, overexpression of wildtype CRY1 hampered

resection only when DNA-PK was active, in agreement with a requirement of DNA-PK-mediated phosphorylation for its anti-resection role (see Suppl. Fig. 4C for representative images). In stark contrast, a CRY1 that cannot be modified by DNA-PK did not impair resection even when DNA-PK was functional. On the contrary, a constitutive phosphorylation of CRY1 was enough to hamper resection even in the presence of DNA-PK inhibitor, reinforcing that these three sites are enough to promote its anti-resection role. To determine the molecular role of those phosphorylation and if these PTMs were affecting CRY recruitment at sites of DSBs, we measured its accumulation at laser-lines in real time in the different CRY1 background (Figure 4D; Suppl. movies 7-9). Strikingly, all three versions of the protein were recruited to DSBs with a similar kinetics. Then, we tested if retention of CRY1 was affected by DNA-PK-mediated phosphorylation by analysing laser lines with longer time courses (Figure 4E; Suppl. movies 10-12) Strikingly, we observed that albeit all three CRY1 variants were readily recruited, only when CRY1 was phosphorylated it was retained at sites of damaged DNA. Thus, these data suggest that upon the appearance of DSBs CRY1 is recruited to sites of broken chromosomes, but only when is then phosphorylated by DNA-PK it is retained. This retention in turn locks CCAR2 onto sites of broken chromosomes, thus creating an anti-resection environment by restraining CtIP.

Circadian regulation of DSB repair affects cell survival to genotoxic agents

Because of CRY1 regulating DNA end resection and, therefore, HR, cells become hyper-resistant to several DNA damaging agents when this factor was depleted (Fig. 5A-B) and hyper-sensitive when it was stabilized using KL001 (Fig. 5C-D). So, we conclude that HR stimulation when CRY1 was low facilitated repair, whereas high CRY1 induced a reduction in HR that hampered DNA repair. Indeed, CRY1 depletion reduced the number of cells with micronuclei 24 h after irradiation with 10 Gy (Fig. 5E; see Suppl. Fig. 5A for representative images) and the number of unrepaired breaks in the next mitosis upon DSB induction (Fig. 5F; see Suppl. Fig. 5B for representative images). On the contrary, stabilization of CRY1 increases the number of unrepaired breaks in the following mitosis after exposure to IR (Fig. 5G; see Suppl. Fig. 5C for representative images). Moreover, when we measured the disappearance of γH2AX 24h after irradiation as a proxy of DSB repair completion, we observed that cells depleted of CRY1 were more efficient than control cells (Fig. 5H; see Suppl. Fig. 5D for representative images). Thus, we conclude that the levels of CRY1 are important to maintain the stability of the genome.

CRY1 presence affects tumour biology and prognosis

Circadian proteins are commonly deregulated in tumour samples. Thus, we wondered if such relationship with the repair of induced DSBs and genomic instability was maintained in those pathological setups and, furthermore, if it could be exploited in the clinic. First, we reasoned that if CRY1 levels impact genomic instability it might affect the probability to acquire secondary mutations in cancer samples that leads to a new tumour event. Indeed, using Pan-Cancer data from The Cancer Genome Atlas (TCGA) we observed that cells with low levels of CRY1, i.e., with and increased recombination capacity and better repair according to our data, showed a delay in the appearance of a new tumour event (Fig. 5I). Then, we reasoned that despite this increase mutagenicity of cancer samples high levels of CRY1, this reduced repair ability can be exploited by using therapeutic agents designed to create DSBs. Indeed, using again TCGA data we were able to analyse the impact of radiotherapy in breast cancer regarding the levels of CRY1. We observed that patients with tumors expressing higher CRY1 levels were more responsive to radiotherapy, in agreement with the idea that high CRY1 levels render the tumour cells more sensitive to radiation (Fig. 5J). On the contrary, breast tumors with lower CRY1 expression were less efficiently treated with radiotherapy (Fig. 5J), with a decrease in the median survival of 1.5 years (571 days). Strikingly, similar results were observed regarding CCAR2 levels (Fig. 5K), albeit with an even bigger increase in median survival of over 2.5 years (957 days), reinforcing that both CCAR2 and CRY1 work in a similar way.

Then, we reasoned that if CRY1 levels affected the response to radiotherapy, it is possible that the time of the day when patients are irradiated might impact the efficiency of this treatment. In a retrospective analysis using patient data from the Radiotherapy Service from the University Hospital Virgen Macarena we analysed this response stratifying the patients in two groups: those irradiated in the morning versus those irradiated in the afternoon/evening. Using Pan-Cancer data we observed a very small but statistically significant difference between those two groups (Fig. 5L). In agreement with our CRY1 levels results, irradiation in the afternoon, when CRY1 levels build up, rendered tumour samples more sensitive to radiotherapy and increase very mildly patient prognosis. We hypothesized that this effect might be very small because many cancers show deregulation of circadian proteins, and in this case, patients might not benefit from this chronotherapy. For example, directly deregulation of CRY1 has been observed in

some tumours such as lung cancer, whereas in other tumour types like prostate cancer deregulation of circadian rhythms does not rely in changes CRY1 levels (Mocellin et al., 2018). Strikingly, careful examination of the data agreed with this idea and, indeed, whereas prostate cancer patients do benefit of specific times of irradiation (Fig. 5M), lung cancer patients did not (Fig. 5N).

DISCUSSION

Circadian rhythms and the repair of DNA damage are strongly evolutionary linked. Indeed, CRY1 belongs to the Cryptochrome family, in which bacterial photolyases are included (Öztürk et al., 2007). Similarly, Timeless acts as a bona fide circadian accessory factor in Drosophila, whereas in mammals has shifted its role toward a checkpoint function (Mazzoccoli et al., 2016). Strikingly, in Drosophila there is a second family member, Timeout, that has been related to the repair of DSBs (Mazzoccoli et al., 2016). So, it seems that during evolution a bleeding between circadian-repair proteins has occurred multiple times. Although this simply crossing between circadian-repair pathways might explain why in mammals CRY1 behaves as both a circadian and a repair factor, a more intriguing hypothesis is that this dual nature reflects an evolutionary benefits of synchronizing DSB repair with the night/day cycle. So, a likely explanation is that this regulation prepares cells to face a load of DSBs at specific times of the day. Considering that UV light is a strong inductor of DNA damage, including DSBs when not repaired by the NER, this connection might not seem surprising. Indeed, NER has been clearly showed to be regulated by the circadian clock, attuning this repair pathway to the part of the day in which UV-derived DNA lesions will appear (Bee et al., 2015). So, a possibility is that this connection reflects a need to prepare cells to face unrepaired UV-lesions that can lead to DSBs that are more likely to appear during the day. However, we do not favour this idea, mostly by two facts. First, most mammalian cells do not suffer this kind of damage as they are protected from the mutagenic effect of UV by the skin. And second and more importantly, we have observed a conservation of the role of CRY1 in mice that disagrees with this hypothesis. Relevantly, mice are nocturnal animals, so they have a 12-hour shift in their circadian clock respect to humans and other diurnal mammals, with CRY1 peaking at dawn and sporting a maximal reduction at dusk (Wang et al., 2017). That means that in mice cells recombination is peaking at dusk and it is reduced at dawn, opposite to what happens in human cells. So, for mice to maintain the

same CRY1-dependent circadian regulation points out toward a different source of DNA damage that does not appear during the day but accumulates at night. An alternative explanation will be replication-borne damage. It has been established that the circadian clock and the cell cycles are in phase, and in human cells that means that replication takes usually place at specific times of the day (Masri et al., 2013). Albeit it is not completely clear how this coordination works, and the time of the day in which replication takes place varies among different cell types, it has been proposed that replication only takes place at specific times (gates) of the day in specific circadian windows (gating model; (Masri et al., 2013)). So, it is possible that the regulation of resection by CRY1 levels is a way to reinforce the cell cycle regulation of homologous recombination, ensuring that resection and HR only happen in specific circadian windows too. A better understanding on the synchronization between replication and the circadian clock is required to test this idea. However, considering all our data together, we favour a different explanation. Indeed, we propose that this circadian synchronization might prepare mammalian cells to a source of damage that is more likely to appear during the day in humans and at night in mice. So, we hypothesize that this circadian regulation might reflect a need to attune DSB repair with the appearance of damage caused by the cellular metabolism, another well-stablished source of DNA damage (Moretton and Loizou, 2020). Interestingly, CCAR2 has been proposed to coordinate the cell metabolism with the circadian clock through its interaction with the Rev-erbα receptor (Chini et al., 2013), suggesting that it might mediate also further coordination of these two aspects with DSB repair. In this model, during the more active phase of the cells, i.e., when the metabolism is more active, higher rates of recombination will be required. So, in humans, cells will benefit of a boost of recombination at dawn whereas mice will favour such increase at dusk as a preparation of the initiation of the active phase of their circadian cycle. Then, during this more active phase recombination can slowly decline until dusk (in human) or dawn (mice) in readiness for a more reduced metabolic status, meaning that the chances of encounter DSBs that require recombination for repair are reduced. Then, the cells will increase slowly again their ability to activate resection to face the next day/night cycle.

But how does this circadian regulation impinge on the regulation of DNA end resection? We favour a model in which is the specific presence of CRY1, and not other circadian factors, what controls resection through CCAR2 and its inhibition of CtIP. Strikingly, this cryptochrome paralogue specificity might reflect the lack of conservation

of the C-terminal tail between CRY1 and CRY2, including the absence of the DNA-PK phosphorylation sites in the later. In our model (Fig. 6; this reflects the circadian regulation in humans, but in mice it will be shifted 12 hours), we envision that the levels of CRY1 are critical to retain CCAR2 and restrain CtIP by a physical interaction between these proteins. Indeed, we think that at dawn (Figure 6, top left) CCAR2 and CtIP are recruited together to DSBs as previously proposed (López-Saavedra et al., 2016). But in the absence of CRY1, CCAR2 cannot stay on damaged DNA, so it is readily evicted from chromatin unleashing CtIP and creating a pro-resection environment. On the contrary, at sunset (Figure 6, bottom left), CRY1 will be constitutively interacting with CCAR2. Therefore, when a DSB appear all three proteins will be recruited on chromatin in a very rapid response. Then, the activation of DNA-PK will cause the phosphorylation of CRY1, what will lock it on DNA, fastening CCAR2 also on the broken chromatin and constraining CtIP activity, most likely acting as a downstream effector of the Shieldin complex as recently described (Iyera et al., 2022). During either the day or the night (Figure 6, right side), cells will react differently depending on the levels of CRY1 that will be accumulating (during the day) or decreasing (during the night), so the breaks will be more or less likely to be resected depending on the CRY1 levels at that specific time of the day.

This built-in mechanism will act at the cellular level. However, there is a secondary control of the circadian rhythms at the level of light sensing that can reset the cellular clock, that in the case of the mammals require the detection of light by the eyes, the processing of this signal at the suprachiasmatic nucleus (SCN), and then the transmission of this information to all the cells in the organism (Stratmann and Schibler, 2006). How this supracellular regulation impinges in this regulatory network we have uncovered should be explored in the future. Indeed, our data suggest that perturbations of the circadian rhythms might have consequences in the ability of the cells to repair broken chromosomes. Furthermore, it will affect not only their ability to repair DSBs, but also the balance between the more error-free HR and the error-prone NHEJ, hence putatively impacting both the quantity and quality of the repair. This might, in turn, affect the stability of the genome, altering the mutational load. Strikingly, it has been known for decades that people that alternate between different day-night shifts at work or suffering of chronic jetlag are more prone to develop cancer and they generally have a poorer prognosis (Lamia, 2017; Shostak, 2017), albeit the reasons are far from clear. One tantalizing idea is that these workers have a deregulation between their DSBs repair

pathways due to the circadian perturbations, so they have a higher chance toward a mutagenic repair that might contribute, among other factors, to tumour development. Along the same lines, the same explanation can be invoked to understand why circadian regulators are often altered in many cancer cells (Xiang et al., 2018; Yu et al., 2013). So, tampering with the built-in circadian clock, either by external effects, such as shift changes, or internal causes, such as mutation of circadian genes, will contribute to an increase in the mutagenic burden that can predispose toward the appearance of cancer. Our own data using TCGA data support this idea of higher chances of tumour development when CRY1 protein levels are reduced. Interestingly, this same weakness that might contribute to the genesis of the cancer can be exploited for their treatment, as cells depleted for CRY1 are sensitive to DSB-inducing agents. The exploitation of the connection between circadian rhythms and cancer treatment efficiency is known as chronotherapy (Lévi, 2001), and there is discussion if this might be applied to radiotherapy (Chan et al., 2017). We have even observed this effect in a real-life clinical setup, albeit with a very modest impact and, interestingly, only on specific tumour samples. Strikingly, those known to accumulate CRY1 alterations, such as lung cancers (Mocellin et al., 2018), do not readily react to the time of irradiation, but those that also accumulate circadian mutations but not in CRY1, such as prostate tumours (Mocellin et al., 2018), do profit. We postulate that a stratification of the patients according to its CRY1 level in combination with a time-specific irradiation might show even better and encouraging results in the clinical practice. Indeed, according to our model, patients in which their cancer cells retain the CRY1 will benefit strongly of an afternoon-evening irradiation due to an increase sensitivity of the cells to DSBs by cause of a reduced HR. On the other hand, a time-specific irradiation of tumors that have lost CRY1 regulation might seems irrelevant. However, we propose that in this case a morning irradiation might be recommended, not because the tumour itself will be especially sensitive, but because the neighbouring tissue will be more resistant, reducing unwanted secondary effects. So, we hypothesize that those cancer that have lost CRY1 regulation should be irradiated during the morning and those that retain CRY1 oscillations during the afternoon. The same rationale can be applied, in principle, to any DSB-inducing chemotherapeutic. However, in that case, a profound knowledge of the pharmacodynamics of the drug would be necessary to synchronize the moment in which the chemotherapeutic agent is causing the DNA breaks with the night/day cycle.

REFERENCES

Baggs, J.E., Price, T.S., Ditacchio, L., Panda, S., Fitzgerald, G.A., and Hogenesch, J.B. (2009). Network features of the mammalian circadian clock. PLoS Biol. *7*, 0563–0575.

Balsalobre, A., Brown, S.A., Marcacci, L., Tronche, F., Kellendonk, C., Reichardt, H.M., Schutz, G., and Schibler, U. (2000). Resetting of circadian time in peripheral tissues by glucocorticoid signaling. Science (80-.). *289*, 2344–2347.

Bee, L., Marini, S., Pontarin, G., Ferraro, P., Costa, R., Albrecht, U., and Celotti, L. (2015). Nucleotide excision repair efficiency in quiescent human fibroblasts is modulated by circadian clock. Nucleic Acids Res. *43*, 2126–2137.

Bhadra, U., Thakkar, N., Das, P., and Pal Bhadra, M. (2017). Evolution of circadian rhythms: from bacteria to human. Sleep Med. *35*, 49–61.

Brown, S.A., Kowalska, E., and Dallmann, R. (2012). (Re)inventing the Circadian Feedback Loop. Dev. Cell *22*, 477–487.

Cejka, P. (2015). DNA end resection: Nucleases team up with the right partners to initiate homologous recombination. J. Biol. Chem. *290*, 22931–22938.

Chan, S., Rowbottom, L., McDonald, R., Bjarnason, G.A., Tsao, M., Danjoux, C., Barnes, E., Popovic, M., Lam, H., DeAngelis, C., et al. (2017). Does the Time of Radiotherapy Affect Treatment Outcomes? A Review of the Literature. Clin. Oncol. *29*, 231–238.

Chang, H.H.Y., Pannunzio, N.R., Adachi, N., and Lieber, M.R. (2017). Non-homologous DNA end joining and alternative pathways to double-strand break repair. Nat. Rev. Mol. Cell Biol. *18*, 495–506.

Chapman, J.R., Barral, P., Vannier, J.B., Borel, V., Steger, M., Tomas-Loba, A., Sartori, A.A., Adams, I.R., Batista, F.D., and Boulton, S.J. (2013). RIF1 Is Essential for 53BP1-Dependent Nonhomologous End Joining and Suppression of DNA Double-Strand Break Resection. Mol. Cell *49*, 858–871.

Chini, E.N., Chini, C.C.S., Nin, V., and Escande, C. (2013). Deleted in breast cancer-1 (DBC-1) in the interface between metabolism, aging and cancer. Biosci. Rep. *33*, 637–643.

Escribano-Díaz, C., Orthwein, A., Fradet-Turcotte, A., Xing, M., Young, J.T.F., Tkáč, J., Cook, M.A., Rosebrock, A.P., Munro, M., Canny, M.D., et al. (2013). A Cell Cycle-Dependent Regulatory Circuit Composed of 53BP1-RIF1 and BRCA1-CtIP Controls DNA Repair Pathway Choice. Mol. Cell *49*, 872–883.

Ferretti, L.P., Lafranchi, L., and Sartori, A.A. (2013). Controlling DNA-end resection:

A new task for CDKs. Front. Genet. *4*, 1–7.

Gao, P., Yoo, S.H., Lee, K.J., Rosensweig, C., Takahashi, J.S., Chen, B.P., and Green, C.B. (2013). Phosphorylation of the cryptochrome 1 C-terminal tail regulates circadian period length. J. Biol. Chem. *288*, 35277–35286.

Gaucher, J., Montellier, E., and Sassone-Corsi, P. (2018). Molecular Cogs: Interplay between Circadian Clock and Cell Cycle. Trends Cell Biol. *28*, 368–379.

Hirota, T., Lee, J.W., St. John, P.C., Sawa, M., Iwaisako, K., Noguchi, T., Pongsawakul, P.Y., Sonntag, T., Welsh, D.K., Brenner, D.A., et al. (2012). Identification of small molecule activators of cryptochrome. Science (80-.). *337*, 1094–1097.

Iyera, D.R., Haradaa, N., Clairmonta, C., Jianga, L., Martignettia, D., Nguyena, H., Hea, Y.J., Chowdhurya, D., and D'Andreaa, A.D. (2022). CCAR2 functions downstream of the Shieldin complex to promote double-strand break end-joining. Proc. Natl. Acad. Sci. *119*, e2214935119.

Izumo, M., Sato, T.R., Straume, M., and Johnson, C.H. (2006). Quantitative analyses of circadian gene expression in mammalian cell cultures. PLoS Comput. Biol. *2*, 1248–1261.

Jackson, S.P., and Bartek, J. (2009). The DNA-damage response in human biology and disease. Nature *461*, 1071–1078.

Jasin, M., and Rothstein, R. (2013). Repair of strand breaks by homologous recombination. Cold Spring Harb. Perspect. Biol. *5*.

Lamia, K.A. (2017). Ticking time bombs: connections between circadian clocks and cancer. F1000Research *6*, 1910.

Lévi, F. (2001). Circadian chronotherapy for human cancers. Lancet Oncol. *2*, 307–315.

Lopez-Saavedra, A., Gomez-Cabello, D., Dominguez-Sanchez, M.S., Mejias-Navarro, F., Fernandez-Avila, M.J., Dinant, C., Martinez-Macias, M.I., Bartek, J., and Huertas, P. (2016). A genome-wide screening uncovers the role of CCAR2 as an antagonist of DNA end resection. Nat. Commun. *7*, 12364.

López-Saavedra, A., Gómez-Cabello, D., Domínguez-Sánchez, M.S., Mejías-Navarro, F., Fernández-Ávila, M.J., Dinant, C., Martínez-Macías, M.I., Bartek, J., and Huertas, P. (2016). A genome-wide screening uncovers the role of CCAR2 as an antagonist of DNA end resection. Nat. Commun. *7*.

Magni, M., Buscemi, G., and Zannini, L. (2018). Cell cycle and apoptosis regulator 2 at the interface between DNA damage response and cell physiology. Mutat. Res. - Rev.

Mutat. Res. *776*, 1–9.

Makharashvili, N., and Paull, T.T. (2015). CtIP: A DNA damage response protein at the intersection of DNA metabolism. DNA Repair (Amst). *32*, 75–81.

Masri, S., Cervantes, M., and Sassone-Corsi, P. (2013). The circadian clock and cell cycle: Interconnected biological circuits. Curr. Opin. Cell Biol. *25*, 730–734.

Mazzoccoli, G., Laukkanen, M.O., Vinciguerra, M., Colangelo, T., and Colantuoni, V. (2016). A Timeless Link Between Circadian Patterns and Disease. Trends Mol. Med. *22*, 68–81.

Mocellin, S., Tropea, S., Benna, C., and Rossi, C.R. (2018). Circadian pathway genetic variation and cancer risk: Evidence from genome-wide association studies. BMC Med. *16*, 1–8.

Moretton, A., and Loizou, J.I. (2020). Interplay between cellular metabolism and the dna damage response in cancer. Cancers (Basel). *12*, 1–29.

Mozaffari, N.L., Pagliarulo, F., and Sartori, A.A. (2021). Human CtIP: A 'double agent' in DNA repair and tumorigenesis. Semin. Cell Dev. Biol. *113*, 47–56.

Öztürk, N., Song, S.H., Özgür, S., Selby, C.P., Morrison, L., Partch, C., Zhong, D., and Sancar, A. (2007). Structure and function of animal cryptochromes. Cold Spring Harb. Symp. Quant. Biol. *72*, 119–131.

Ranjha, L., Howard, S.M., and Cejka, P. (2018). Main steps in DNA double-strand break repair: an introduction to homologous recombination and related processes. Chromosoma *127*, 187–214.

Shostak, A. (2017). Circadian clock, cell division, and cancer: From molecules to organism. Int. J. Mol. Sci. *18*.

Stratmann, M., and Schibler, U. (2006). Properties, entrainment, and physiological functions of mammalian peripheral oscillators. J. Biol. Rhythms *21*, 494–506.

Symington, L.S. (2016). Mechanism and regulation of DNA end resection in eukaryotes. Crit. Rev. Biochem. Mol. Biol. *51*, 195–212.

Takahashi, J.S. (2017). Transcriptional architecture of the mammalian circadian clock. Nat. Rev. Genet. *18*, 164–179.

Di Virgilio, M., Callen, E., Yamane, A., Zhang, W., Jankovic, M., Gitlin, A.D., Feldhahn, N., Resch, W., Oliveira, T.Y., Chait, B.T., et al. (2013). Rif1 prevents resection of DNA breaks and promotes immunoglobulin class switching. Science (80-.). *339*, 711–715.

Wang, J., Mauvoisin, D., Martin, E., Atger, F., Galindo, A.N., Dayon, L., Sizzano, F.,

Palini, A., Kussmann, M., Waridel, P., et al. (2017). Nuclear Proteomics Uncovers Diurnal Regulatory Landscapes in Mouse Liver. Cell Metab. *25*, 102–117.

Xiang, R., Cui, Y., Wang, Y., Xie, T., Yang, X., Wang, Z., Li, J., and Li, Q. (2018). Circadian clock gene Per2 downregulation in non-small cell lung cancer is associated with tumour progression and metastasis. Oncol. Rep. *40*, 3040–3048.

Yu, H., Meng, X., Wu, J., Pan, C., Ying, X., Zhou, Y., Liu, R., and Huang, W. (2013). Cryptochrome 1 Overexpression Correlates with Tumor Progression and Poor Prognosis in Patients with Colorectal Cancer. PLoS One *8*.

ACKNOWLEDGEMENTS.

We thank Andrés J. López-Contreras and José Carlos Reyes-Rosa for critical reading of the manuscript. This work was funded by the R+D+I grant PID2019-104195G from the Spanish Ministry of Science and Innovation-Agencia Estatal de Investigación/10.13039/501100011033 and the grant P18-RT-1204 from the Consejería de Transformación Económica, Industria, Conocimiento y Universidades, Junta de Andalucía. AR-F is funded with a FPU fellowship from the Spanish Ministry of Education and MC-P is the recipient of a MSCA-IF-2020 (coDNAres). CABIMER is supported by the regional government of Andalucía (Junta de Andalucía).

DATA AVAILABILITY.

All relevant data are included in the manuscript. Raw data will be provided upon request.

FIGURE LEGENDS

Figure 1. Resection oscillates following a circadian pattern. A, Schematic representation of the experimental setup for circadian synchronization. Cells were exposed to dexamethasone or forskolin for two hours. Then, cells were released by changing the medium, mimicking sunrise conditions. Cells were then irradiated at the indicated timepoints that correspond to the depicted times of the day/night cycle. **B**, U2OS were synchronized as mentioned in A with either Dexamethasone (blue line) or EtOH as a control (red line) and irradiated with 10Gy at the indicated time points. 1 h later cells were immunostained for RPA. Then, the percentage of cells with more than 10 RPA foci was scored. Statistically significance was calculated using a two-way ANOVA. Only statistical different comparisons are depicted. **C**, Same as B, but using Forskolin (blue line) or DMSO as a control (red line). **D**, Same as B but in RPE1 cells. Dashed line represents the value of an asynchronous control. **E**, Same as D but in MEFs. **F**, The length of resected DNA was calculated as described in the methods section in cells synchronized and released from dexamethasone at the indicated times or in an asynchronous control. Each dot represents the length of an individual resected DNA fiber, and the median is shown in red. Statistical significance was calculated using an Mann–Whitney test. The experiment was repeated three times with similar results. **G**, Same as D but immunostaining for BRCA1. **H**, Same as D but immunostaining for RIF1. **I**, Same as D but immunostaining for RAD51 3 hours after DSB induction with IR. Unless stated otherwise, for all main and supplementary figures, the average and standard deviation of three independent experiments are shown and p values are represented with one ($p < 0.05$), two ($p < 0.01$) or three ($p < 0.001$) asterisks.

Figure 2. Resection oscillates following a circadian pattern. A, CRY1 (siCRY1) or control (siNT) depleted U2OS cells were transfected with the human version of CRY1 (black bars) or an empty vector (white). 1 h after irradiation with 10 Gy cells were immunostained for RPA. Then, the percentage of cells with more than 10 RPA foci was scored (left). Statistically significance was calculated using a two-way ANOVA. Only statistical different comparisons are depicted. Representative images are shown on the right side. **B**, QIBC representation of RPA foci formation. Cells treated as in A were immunostained for RPA. The intensity of RPA or DAPI were plotted in the Y and X axis, respectively. The vertical dashed line represents the threshold of DAPI intensity corresponding to S/G2 cells, whereas the horizontal line represents the threshold for RPA positive cells. The percentage of S/G2 cells showing RPA foci signal is indicated. A

representative experiment out of 2 two independent replicates is shown. **C**, Same as A but in cells overexpressing or not CRY1 without siRNA transfection. **D**, Same as A but in cells treated with the CRY1 stabilizer KL001. **E**, Gene conversion was assessed in U2OS cells bearing the DR-GFP reporter in cells transfected with an siRNA against CRY1 (siCRY1) or a control sequence (siNT), as indicated. The amount of GFP positive cells, i.e., cells that have undergone repair by gene conversion, after induction with the nuclease I-SceI, were normalized to the siNT control taken as 1. The statistical significance was calculated using a Student´s t-test. **F**, Same as E, but using the SSA reporter SA-GFP. **G**, Same as E, but using the SSA reporter EJ5-GFP. **H**, Same as E, but in cells bearing an empty vector or a vector harboring an ectopic version of CRY1. **I**, Same as H, but using the SSA reporter SA-GFP. **J**, RAD51 foci 3 hr after exposure to irradiation were scored by immunofluorescence in cells depleted for CRY1 (siCRY1) or control cells (siNT). The number of RAD51 foci per cell was counted and represented as a single dot. The median number of Rad51 foci is shown as a red line. Statistical significance was calculated using a Mann–Whitney test. A representative experiment out of three with similar results is shown. **K**, Same as J, but in cells transfected with a plasmid bearing an ectopic copy of CRY1 or an empty vector. **L**, Same as J, but immunostaining for RIF1. **M**, Same as L, but in cells transfected with a plasmid bearing an ectopic copy of CRY1 or an empty vector.

Figure 3. CRY1 levels control DNA end resection through CCAR2 retention at DSBs. **A**, U2OS bearing shRNA against CCAR2 (shCCAR2), CtIP (shCtIP) or a control sequence (shNT), were synchronized and released as indicated in Figure 1A with dexamethasone. Cells were irradiated at the indicated time points and RPA foci were scored by immunostaining 1 h after irradiation. Statistically significance was determined using a two-way ANOVA. Statistical differences between shRNAs are marked in black, whereas differences in the same cell line at different time points are shown in the designated color. **B**, RPA foci formation in U2OS cells transfected with the indicated siRNAs. A minus sign means transfection with a control sequence. **C**, Same ad B, but in cells transfected with a siRNA against CCAR2 or not and bearing a vector for CRY1 overexpression (hCRY1). Minus signs means transfection with a siRNA control or the empty vector. **D**, U2OS cells were irradiated with 10G (+) or mock treated (-). Protein samples were isolated in native condition and CRY1 was immunoprecipitated using a specific antibody. IgG was used as immunoprecipitation control. Then, proteins were

resolved in SDS PAGE and blotted with the indicated antibodies. **E**, Same as D but in cells depleted for CtIP using a siRNA. **F**, U2OS cells bearing Cherry-MDC1 and GFP-CRY1 constructs were laser microirradiated and imaged at the indicated times. Representative images of selected timepoints are shown on the right, and quantification of the signal, relative to the peak intensity taken as 100%, of 6 cells is represented on the right. **G**, U2OS cells transfected with a siRNA against CRY1 or a control sequence were irradiated with 10 Gy. Protein samples were taken at the indicated timepoints, and the chromatin fraction was purified. After resolving the sample in SDS PAGE, the amount of phosphorylated CCAR2 was determined using a specific antibody. Lamin A was used as a control. A representative western blot, out of three with similar results, is shown on the left and its quantification of this specific western blot on the right. **H**, U2OS cells treated as in G were immunostained using an antibody against phosphorylated CCAR2. Representative images are shown on the left side, and the quantification of the phospo-CCAR2 intensity per cell is plotted on the right side in cells irradiates (IR +) or not (IR -). **I**, U2OS cells bearing a constitutively expressed CCAR2-GFP fusion were laser microirradiated. The percentage of cells showing a negative GFP staining 1 h after laser-microirradiated was quantified and plotted (right side) in cells depleted or not for CRY1. Representative image of a cell showing an anti-stripe (white arrow) before and 1 h after laser-microirradiation are also shown (left). **J**, The intensity of CCAR2-GFP at the anti-stripe of cells showing them was calculated, setting the pan-nuclear intensity as 0, in U2OS cells laser-microirradiated upon depletion of CR1 or CtIP. The average intensity in each case is shown as a red line. At least 60 cells with anti-stripes were analyzed in each sample. **K**, Recruitment of GFP-CtIP was measure upon laser microirradiation in U2OS cells transfected with an siRNA against CRY1 or a control sequence. Representative images are shown on the left side. Images were taken at the indicated times, and the intensity of GFP-CtIP at the laser-induced stripe was quantified and plotted. **L**, Same as K, but in cells stably expressing a Cherry-CtIP and transfected with a GFP-CRY1 plasmid or an empty vector.

Figure 4. DNA-PK-dependent phosphorylation of CRY1 modulates resection. A, U2OS cells were exposed to the CRY1 stabilizer KL001 and/or the DNA-PK inhibitor NU7441 as indicated with the plus and minus signs, and then irradiated and immunostained for RPA. **B**, Same as A but in cells transfected with an ectopic version of CRY1 or the empty vector instead of exposed to KL001. **C**, Cells stable transfected with

GFP-fusions of wildtype CRY1 (GFPCRY1-wt), a non-phosphoritable version of CRY1 (GFPCRY1-3A), a phospho-mimicking version (GFPCRY1-3E) or the empty vector (GFP) were treated with NU7441 or not, as indicated, irradiated and immunostained for RPA. **D**, U2OS stably expressing GFP-CRY1 versions were laser microirradiated and imaged at the indicated times. For each timepoint, the average intensity of at least five cell images is plotted. **E**, Same as D.

Figure 5. CRY1 levels modulate the response to DNA damaging agents *in vitro* and in cancer samples. A, U2OS transfected with an siRNA against CRY1 or a control sequence were seeded at low density and irradiated at the indicated dose. Cells were left to grow for 10 days and the survival fraction, compared with an unirradiated sample taken at 100%, is plotted. **B**, Same as A but in cells treated with the indicated doses of etoposide (VP16) for 1 hour. **C**, Same as A but in cells pre-exposed to the CRY1 stabilizer KL001 or DMSO. **D**, Same as B but in cells pre-exposed to the CRY1 stabilizer KL001 or DMSO. **E**, U2OS cells depleted or not of CRY1, as indicated, were irradiated with 10 Gy. 24 h after irradiation cells were stained with DAPI and the percentage of cells with micronuclei was calculated. **F**, Percentage of chromosome breaks present in mitotic cells following an irradiation with 2 Gy in cells transfected with the indicated siRNAs. **G**, Same as F, but in cells exposed to KL001 or DMSO. **H**, Number of γH2AX foci in U2OS cells unchallenged (-) or 24 h after irradiation (+; 10 Gy), in cells transfected with an siRNA against CRY1 (+) or a control sequence (-), as indicated. **I**, Elapsed days for a second tumour event in cells stratified for its CRY1 levels in two categories: High (red line) or low (blue line). Data from TCGA. The number of tumour samples is indicated. **J**, Survival of breast cancer patients treated with radiotherapy according the CRY1 levels of the tumour cells. Data from TCGA. Other details as in I. **K**, Same as J but regarding CCAR2 levels. **L**, Overall survival of cancer patients treated primarily with radiotherapy at the Radiotherapy Service of the University Hospital Virgen Macarena considering if they were irradiated in the morning (blue line) or the afternoon (red line). **M**, Same as L but considering only prostate cancer patients. **N**, Same as L but considering only lung cancer patients.

Figure 6. Schematic representation of CRY1-mediated regulation of DNA end resection regarding the time of the day in human samples. At dawn (top-left), when CRY1 is absent, CtIP and CCAR2 are recruited to DSBs. However, CCAR2 cannot be

maintained into chromatin, releasing CtIP and promoting maximum resection. On the contrary, at dusk (bottom left), CRY1 interacts with CCAR2. Upon DSB formation, all three proteins are recruited to damaged chromatin, where CRY1 is phosphorylated by DNA-PK. This locks CRY1 and, consequently, CCAR2 on chromatin, hampering CtIP activity, During the day (top right) or the night (bottom night), when CRY1 levels fluctuate, an intermediate situation ensues. I. e. some breaks will be promptly resected and some will not, depending on the presence of CRY1.

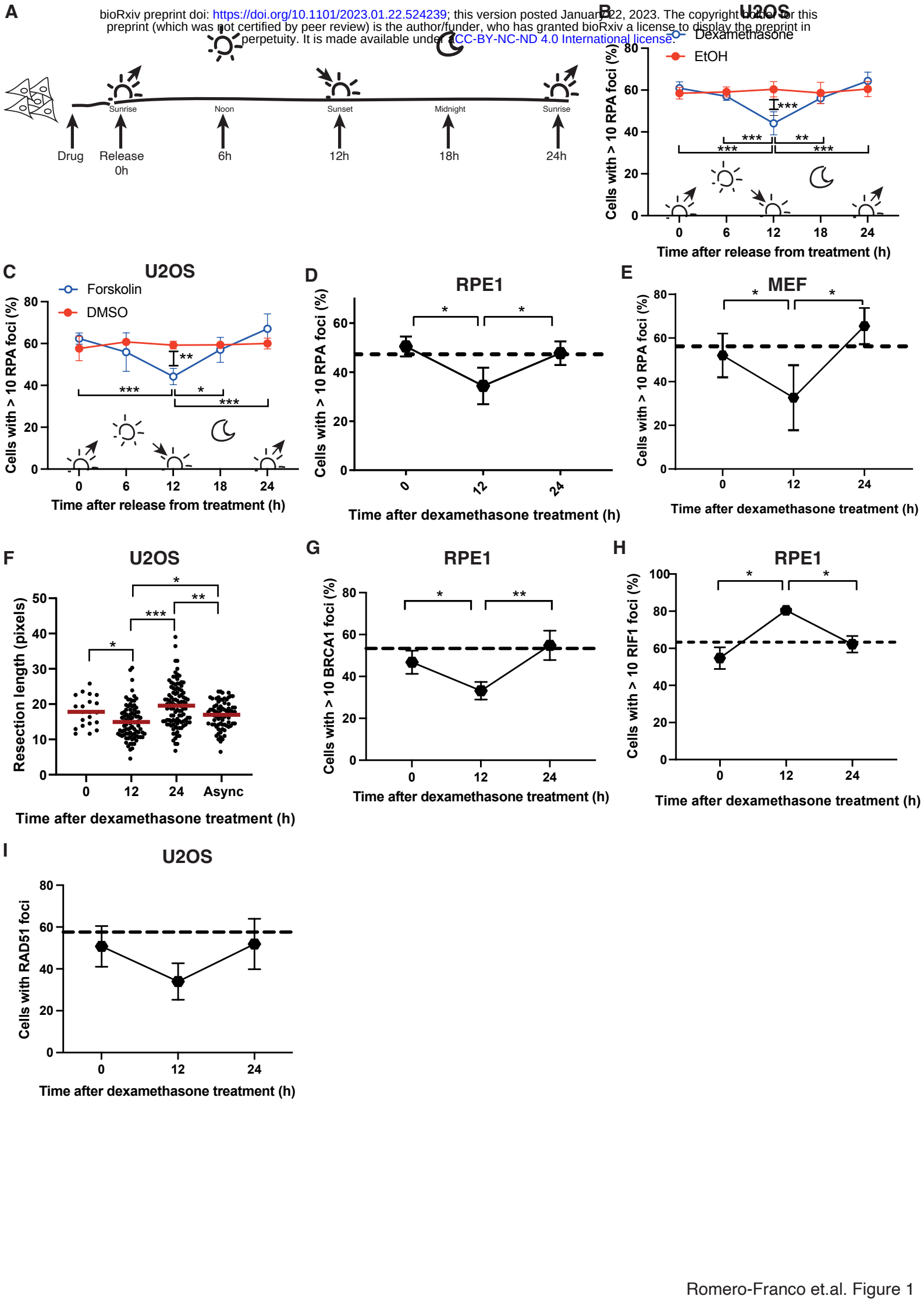

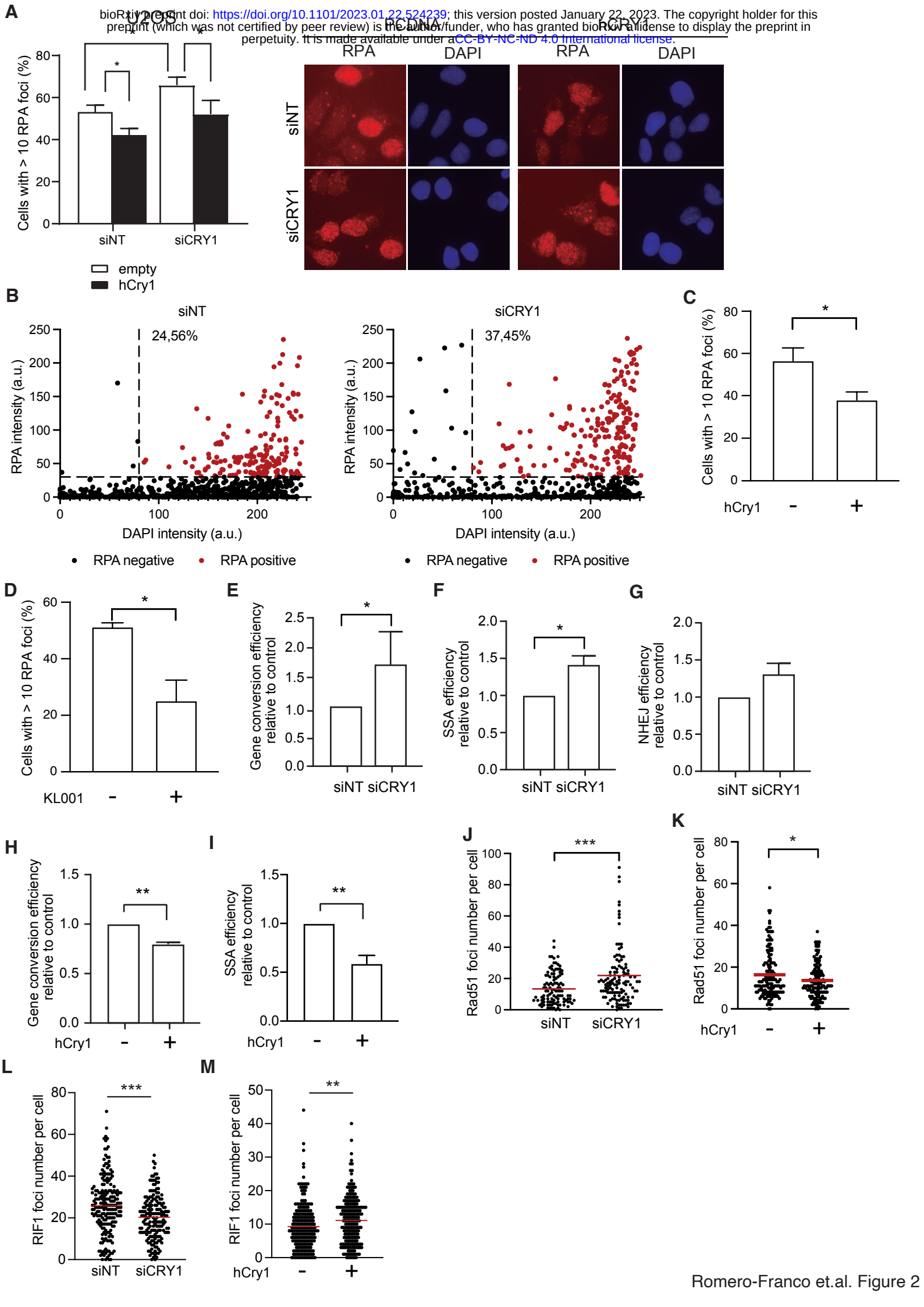

Romero-Franco et.al. Figure 2

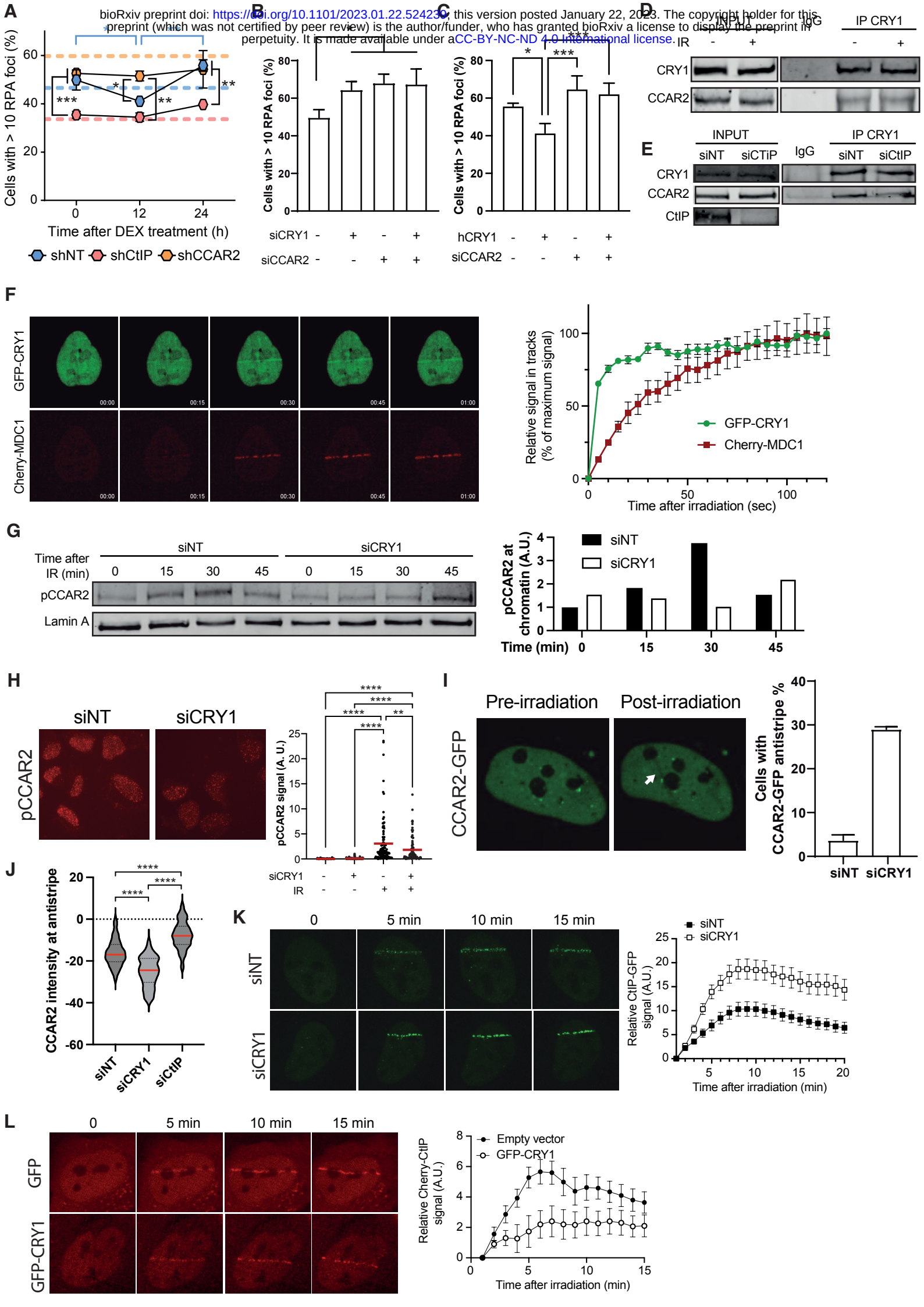

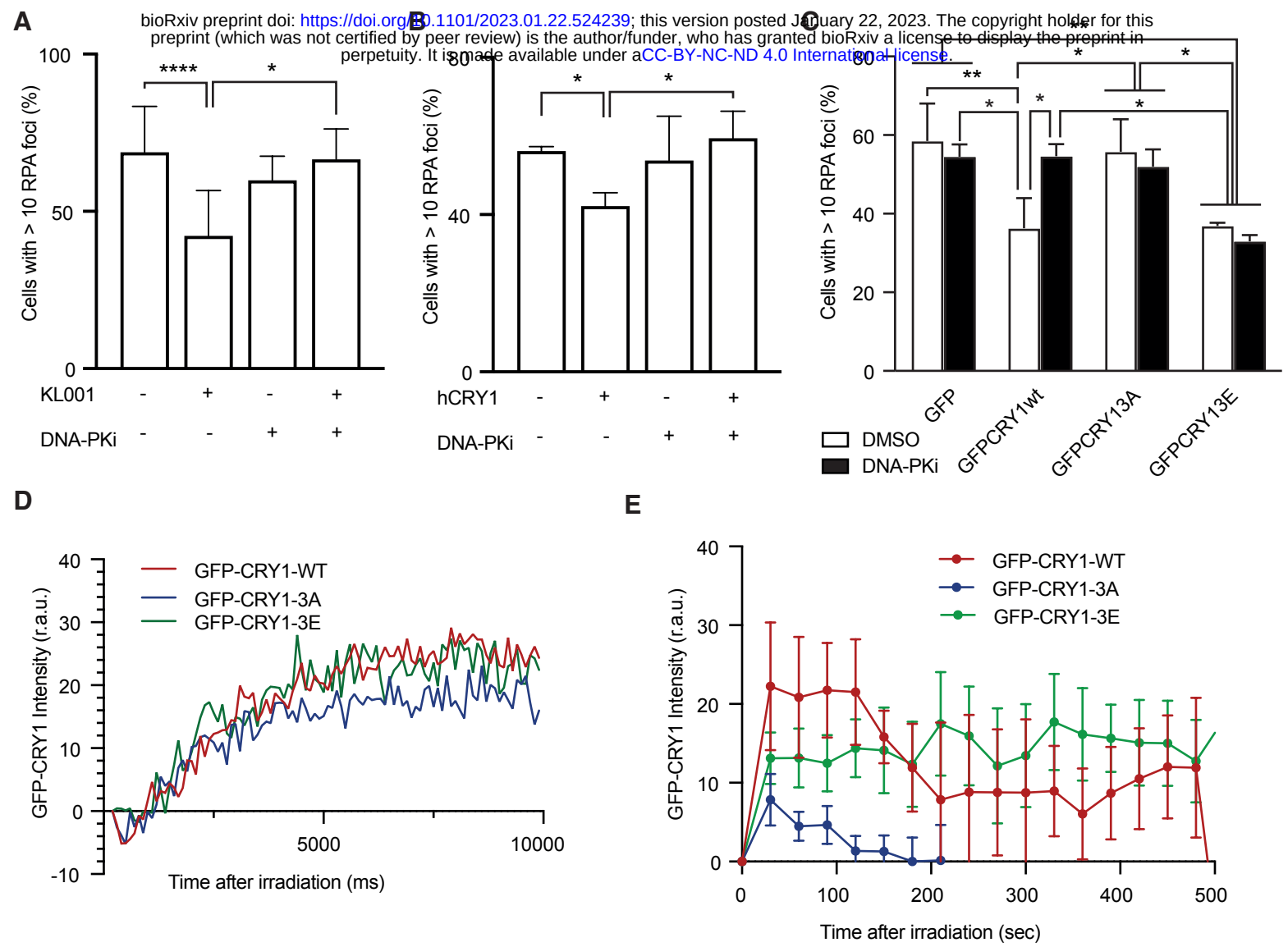

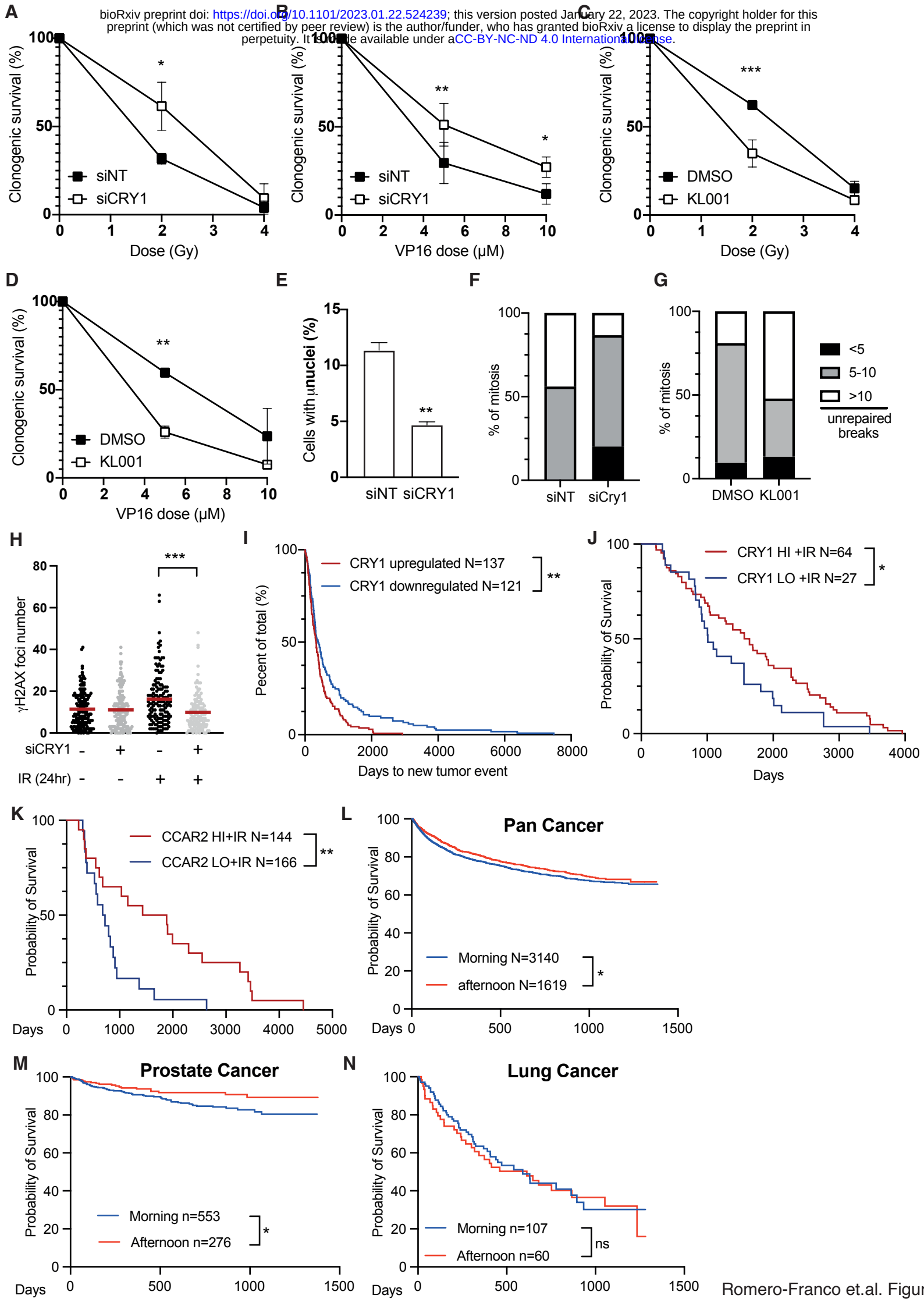

Romero-Franco et.al. Figur

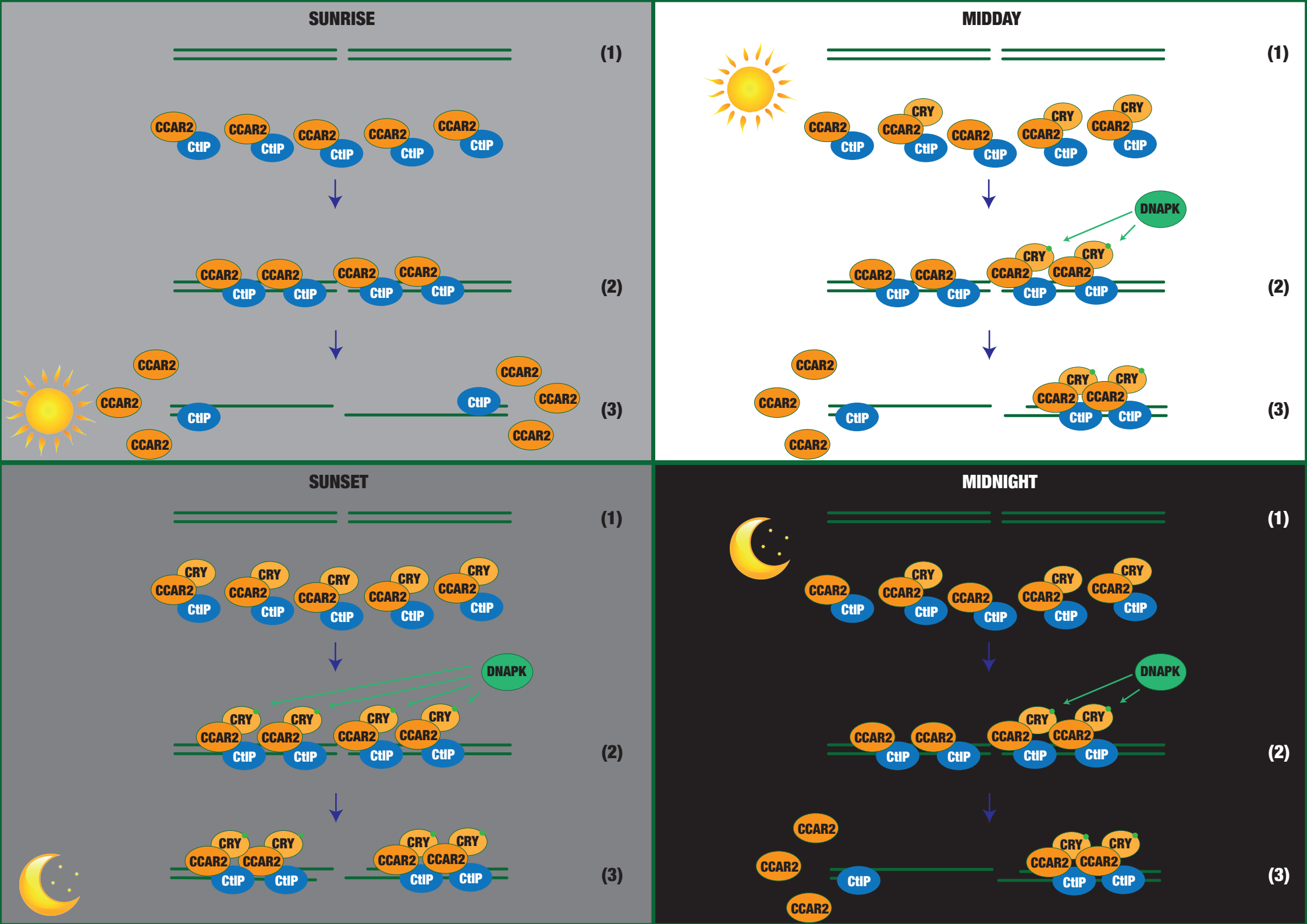
SUNRISE
(1)
CCAR2
CtIP
(2)
(3)
MIDDAY
CRY
DNAPK
SUNSET
MIDNIGHT